6th Annual International IEEE EMBS Conference on Neural Engineering
San Diego, California, 6 - 8 November, 2013

Wavelet-Approximated Generalized Matched Filter for the Detection of Multisensor Extracellular Action Potentials

Agnieszka A. Szymanska[1] and Zoran Nenadic[1,2]

Abstract— **Signal detection represents the first processing step in the analysis of extracellular action potentials (EAPs). By combining the theory of wavelets with statistical signal detection, we derived an approximation of the generalized matched filter that is suitable for semi-supervised (noise known, signal unknown) detection of EAPs in multisensor recordings. When tested on experimental data recorded by a 4-sensor electrode (tetrode), the filter yielded significant signal-to-noise ratio improvements with respect to the original data and several popular multivariate signal processing methods.**

I. Introduction

A great deal of our understanding of neocortical function in awake animals [1] and humans [2] can be attributed to the interpretation of extracellular action potentials (EAPs). Therefore, accurate detection of EAPs is crucial to ensure accurate subsequent processing steps and ultimately correct data interpretation. Detection of EAPs may be challenging due to thermal, quantization, and ambient noise that are imposed by the recording hardware and environment. Biological noise sources, such as EAPs of background neurons, or ion-channel noise [3], are generally correlated with EAPs of interest, further aggravating their detection.

In single-sensor recordings, the above problem can be surmounted by single-unit isolation — a process wherein the recording electrode is placed near a target neuron so that its activity can be separated from noise and the activity of nearby neurons. This yields recordings of high signal-to-noise ratios (SNRs), thus obviating the need for sophisticated EAP detection methods. In multisensor recordings, single-unit isolation may be neither achievable nor desirable, as the array provides sufficient information for multiple EAPs to be disambiguated. Achieving this feat, however, requires the development of appropriate array signal processing tools.

This article presents a rational design approach to building a multisensor EAP detector. The proposed method is rooted in statistical detection theory which is modified to account for scenarios when the signals of interest are not known. Based on biophysical constraints on the duration and shape of EAPs, we argue that the SNR of extracellular recordings can be significantly improved using an appropriate continuous wavelet basis. We also show that *ad hoc* multivariate processing methods may not only fail to improve, but can actually lower the SNR. These points are objectively demonstrated using experimental data recorded by a commercial tetrode.

Work supported by the National Science Foundation (Award #1056105).

[1]Department of Biomedical Engineering, University of California, Irvine, CA 92697, USA {aszymans,znenadic}@uci.edu

[2]Department of Electrical Engineering and Computer Science, University of California, Irvine, CA 92697, USA

II. Background

A. Multisensor EAP Detection

In general, automated approaches to EAP detection can be supervised or unsupervised. Supervised detection assumes that measurements of both EAPs and noise are available before the detector is designed. In a multisensor setup, the best-known representative of these techniques is the matched filter approach by Gozani and Miller [4]. It departs from the classical matched filter approach (see Section II-B) in that it simultaneously maximizes the SNR and minimizes the interference between EAPs to facilitate subsequent EAP classification. However, minimizing the interference between EAPs may compromise their detectability. In addition, this method requires construction of EAP templates, which may be inconvenient especially if the number of recorded neurons is high (a single tetrode in a neuron-dense region may simultaneously record activity from up to 20 neurons [5]).

In unsupervised (blind) detection, noise and EAP templates are generally unknown. However, a similar problem is commonly encountered in approximation theory, where blind signal/noise separation is effectively accomplished in a suitable sparse representation basis [6]. Motivated by these ideas, Nenadic and Burdick [7] applied Bayesian decision theory in a continuous wavelet transform (CWT) domain to develop a fully unsupervised EAP detection algorithm. An extension of this work utilizes probabilistic models to identify EAPs as outliers in a noise distribution [8]. However, both of these methods are only suitable for single-sensor data, and to the best of our knowledge, there are no methods for unsupervised EAP detection in multisensor recordings.

Extracellular recordings often generate measurements that contain no visually discernible EAPs. From this so-called noise-only data, the noise statistics can be estimated and utilized in EAP detection. Falling between the extreme cases above, this approach to EAP detection will be referred to as semi-supervised. In the context of tetrode recordings, power detection [9] and a prewhitening transform [10] are good representatives of this approach. The former method calculates the power of data over a short time segment and compares it to that of background noise. Since the power of EAPs is expected to be above the baseline, a suitable threshold can be defined that separates EAPs from noise [9], [11]. The prewhitening approach, on the other hand, uses the spatial covariance matrix of noise to decorrelate noise samples across channels and normalize their variance to 1. Detection thresholds are then set for each channel in the prewhitened space [10].

978-1-4673-1969-0/13/$31.00 ©2013 IEEE

B. Statistical Detection Theory

The detection of EAPs can be posed as a statistical hypothesis testing problem, where under the null hypothesis, $\mathcal{H}_0$, no EAP is present, and under the alternative, $\mathcal{H}_1$, both an EAP and noise are present. Expressed mathematically, we have:

$$\begin{aligned} \mathcal{H}_0: &\quad \boldsymbol{x}(k) = \boldsymbol{n}(k), \quad k \in \mathcal{L} \\ \mathcal{H}_1: &\quad \boldsymbol{x}(k) = \boldsymbol{s}(k) + \boldsymbol{n}(k), \quad k \in \mathcal{L} \end{aligned} \tag{1}$$

where $\boldsymbol{x} \in \mathbb{R}^{c\times 1}$ is a multisensor measurement, c is the number of sensors, $\boldsymbol{n} \in \mathbb{R}^{c\times 1}$ is zero-mean sensor noise, $\boldsymbol{s} \in \mathbb{R}^{c\times 1}$ is an EAP, and $\mathcal{L} = \{1, 2, \cdots, l\}$, with l being the number of samples spanned by the EAP. Note that due to variability of noise sources (see Section I), $\boldsymbol{n}$ cannot be modeled as spatio-temporally white noise.

To utilize spatio-temporal information, let us organize the measurement matrix $\boldsymbol{X} = [\boldsymbol{x}(1)\, \boldsymbol{x}(2) \cdots \boldsymbol{x}(l)] \in \mathbb{R}^{c\times l}$ into a row vector $\underline{\boldsymbol{x}} = [\boldsymbol{x}_1(\mathcal{L})\, \boldsymbol{x}_2(\mathcal{L}) \cdots \boldsymbol{x}_c(\mathcal{L})] \in \mathbb{R}^{1\times cl}$, where $\boldsymbol{x}_i(\mathcal{L})$ is the ith row of $\boldsymbol{X}$. The optimal decision rule is given by the likelihood ratio test (LRT) [12]:

$$\frac{p(\underline{\boldsymbol{x}}\,|\mathcal{H}_1)}{p(\underline{\boldsymbol{x}}\,|\mathcal{H}_0)} \underset{\mathcal{H}_0}{\overset{\mathcal{H}_1}{\gtrless}} \gamma, \tag{2}$$

which is understood as "accept $\mathcal{H}_1$ if the ratio exceeds γ, otherwise accept $\mathcal{H}_0$." The threshold γ can be based on either an acceptable false alarm rate (Neyman-Pearson detector), or the relative cost of false alarms and omissions as well as the prior probabilities, $P(\mathcal{H}_0)$ and $P(\mathcal{H}_1)$ (Bayesian detector). In these respective cases, the LRT (2) either maximizes the probability of detection or minimizes the Bayes risk.

Let us assume Gaussian noise $\underline{\boldsymbol{n}} \sim \mathcal{N}(\underline{\boldsymbol{0}}, \boldsymbol{\Sigma})$, where $\underline{\boldsymbol{n}} \in \mathbb{R}^{1\times cl}$ is the row-vector form of the noise matrix, $\boldsymbol{N} = [\boldsymbol{n}(1)\, \boldsymbol{n}(2) \cdots \boldsymbol{n}(l)] \in \mathbb{R}^{c\times l}$, and $\boldsymbol{\Sigma} \in \mathbb{R}^{cl\times cl}$ is the spatio-temporal noise covariance matrix. Under this condition, the test (2) takes the form of a generalized matched filter (GMF):

$$\underline{\boldsymbol{s}}\boldsymbol{\Sigma}^{-1}\underline{\boldsymbol{x}}^{\mathrm{T}} \underset{\mathcal{H}_0}{\overset{\mathcal{H}_1}{\gtrless}} \gamma', \tag{3}$$

where $\underline{\boldsymbol{s}} \in \mathbb{R}^{1\times cl}$ is the row-vector form of the signal matrix, $\boldsymbol{S} = [\boldsymbol{s}(1)\, \boldsymbol{s}(2) \cdots \boldsymbol{s}(l)] \in \mathbb{R}^{c\times l}$, and γ' is the detection threshold that subsumes γ and data-independent terms. Note that the test statistic, $T(\underline{\boldsymbol{x}}) = \underline{\boldsymbol{s}}\boldsymbol{\Sigma}^{-1}\underline{\boldsymbol{x}}^{\mathrm{T}} \in \mathbb{R}$, depends linearly on the data $\underline{\boldsymbol{x}}$. Even if $\underline{\boldsymbol{n}}$ is non-Gaussian, no other linear combination of the data can achieve a SNR as high as $T(\underline{\boldsymbol{x}})$. In this case, though, the performance of the GMF may fall short of the LRT detector [12].

Based on Section II-A, we consider the following cases:

(C1) Samples of both $\underline{\boldsymbol{n}}$ and $\underline{\boldsymbol{s}}$ are available — SNR-optimal detection is achievable based on (3).

(C2) Samples of $\underline{\boldsymbol{n}}$ are available, but those of $\underline{\boldsymbol{s}}$ are not — near SNR-optimal detection should be achievable based on (3) and an appropriate signal model.

(C3) Samples of neither $\underline{\boldsymbol{n}}$ nor $\underline{\boldsymbol{s}}$ are available — it is unclear how to utilize (3), as $\boldsymbol{\Sigma}$ and γ' are generally unknown.

We have thus created a common statistical ground for the supervised, semi-supervised and unsupervised approaches to EAP detection. In this article, we will pursue the case (C2), while noting that the solution to (C1) is straightforward, but may be impractical, and that (C3) remains open ended.

III. Methods

When the signal of interest, $\underline{\boldsymbol{s}}$, is unknown, the performance of the detector (3) depends on signal representation [13]. Our prior work [7], [8] provides extensive arguments for using the CWT of the biorthogonal class for EAP representation. Briefly, the shape of these wavelet functions is reminiscent of the predominantly biphasic shape of many EAPs [14]. Furthermore, since EAPs are highly localized in time with characteristic durations of $\sim$1 ms [14], [15], an extremely large set of CWT scales can be significantly reduced. Finally, the translation invariance of the CWT ensures that the representation of an EAP does not depend on its relative position within the time series. These last two properties of the CWT make it more suitable to EAP detection than the commonly used discrete wavelet transform with dyadic scales and translations [16], [17].

Let $\boldsymbol{\psi}_{a,b}(\mathcal{L}) = [\psi_{a,b}(1)\, \psi_{a,b}(2) \cdots \psi_{a,b}(l)] \in \mathbb{R}^{1\times l}$ be discrete samples of a compactly-supported wavelet function, $\psi_{a,b} \in L^2(\mathbb{R})$, with the scale $a > 0$ and translation b. The approximation of the GMF test statistic, $T(\underline{\boldsymbol{x}})$, at the scale a and translation b is given by:

$$T_{a,b}(\underline{\boldsymbol{x}}) = \underline{\boldsymbol{\psi}}_{a,b} \begin{bmatrix} \boldsymbol{\Sigma}_{1,1} & \boldsymbol{\Sigma}_{1,2} & \cdots & \boldsymbol{\Sigma}_{1,c} \\ \boldsymbol{\Sigma}_{2,1} & \boldsymbol{\Sigma}_{2,2} & \cdots & \boldsymbol{\Sigma}_{2,c} \\ \vdots & \vdots & \ddots & \vdots \\ \boldsymbol{\Sigma}_{c,1} & \boldsymbol{\Sigma}_{c,2} & \cdots & \boldsymbol{\Sigma}_{c,c} \end{bmatrix}^{-1} \underline{\boldsymbol{x}}^{\mathrm{T}} \tag{4}$$

where $\underline{\boldsymbol{\psi}}_{a,b} \in \mathbb{R}^{1\times cl}$ is the row-vector form of the matrix:

$$\boldsymbol{\Psi}_{a,b} = \begin{bmatrix} \boldsymbol{\psi}_{a,b}(\mathcal{L}) \\ \boldsymbol{\psi}_{a,b}(\mathcal{L}) \\ \vdots \\ \boldsymbol{\psi}_{a,b}(\mathcal{L}) \end{bmatrix} \in \mathbb{R}^{c\times l}$$

and the submatrix $\boldsymbol{\Sigma}_{i,i} \in \mathbb{R}^{l\times l}$ is the temporal covariance matrix of noise at sensor i. Similarly, $\boldsymbol{\Sigma}_{i,j} \in \mathbb{R}^{l\times l}$ $(j \neq i)$ is the temporal cross-covariance matrix of noise at sensors i and j. In general, estimating the full covariance matrices may require a prohibitively large noise sample. Assuming wide-sense stationary noise, we obtain submatrices $\boldsymbol{\Sigma}_{i,j}$ $(\forall i, j = 1, 2, \cdots, c)$ in Toeplitz (strip diagonal) form, which reduces the number of parameters from $(l^2 + l)/2$ to l.

Written explicitly, the test statistic (4) becomes: $T_{a,b}(\underline{\boldsymbol{x}}) = \sum_{i=1}^{c} \boldsymbol{h}_{a,b}^{i}\, \boldsymbol{x}_i^{\mathrm{T}}(\mathcal{L})$, where a basis vector, $\boldsymbol{h}_{a,b}^{i} \in \mathbb{R}^{1\times l}$, is defined as:

$$\boldsymbol{h}_{a,b}^{i} = \boldsymbol{\psi}_{a,b}(\mathcal{L}) \sum_{j=1}^{c} \tilde{\boldsymbol{\Sigma}}_{j,i} \quad i = 1, 2, \cdots, c \tag{5}$$

In other words, $T_{a,b}$ is obtained by projecting the ith row of the data matrix $\boldsymbol{X}$ onto $\boldsymbol{h}_{a,b}^{i}$ and summing the projections over sensors. The matrix, $\tilde{\boldsymbol{\Sigma}}_{j,i} \in \mathbb{R}^{l\times l}$, is the submatrix

of $\boldsymbol{\Sigma}^{-1}$ corresponding to the block $\{j,i\}$ [see Eq. (4)]. Note, however, that $\boldsymbol{\Sigma}_{j,i} \neq \boldsymbol{\Sigma}_{j,i}^{-1}$. To process the whole length-t time series, as opposed to a length-l block, we vary translation b over the set $\mathcal{T} = \{0, 1, \cdots, t-1\}$. Alternatively, we can slide the basis vectors (5) sample-by-sample, and at each position, we obtain $T_{a,b}$ by projection and summation over sensors. This is efficiently implemented by flipping the basis vectors $\boldsymbol{h}_{a,b}^{i}$, followed by a convolution with the individual sensor data and summation over sensors. Note that this results in a single-scale test statistic, $T_a(\mathcal{T}) \in \mathbb{R}^{1\times t}$, and that the basis vectors processed in this manner represent the impulse response of a wavelet-approximated generalized matched filter (AGMF).

IV. RESULTS

A. Experimental Data

The data collection process is described in [18]. Briefly, a planar silicon probe [19] consisting of 4 tetrodes was placed beneath the surface of the antennal lobe of an adult locust. Only 20 s of data from one of the tetrodes is publicly available [20]. The signals were amplified, band-pass filtered (300-5,000 Hz), and sampled at 15 kHz.

To objectively measure the SNR, 20 EAPs and 25 noise segments (duration between 10 and 60 ms), were randomly selected and manually delineated in the time series data. Extracting longer noise segments was not possible due to the high firing rates of the neurons (see Fig. 1). Note that these noise samples were used to design the basis vectors (5), whereas the sole purpose of the EAPs was for validation.

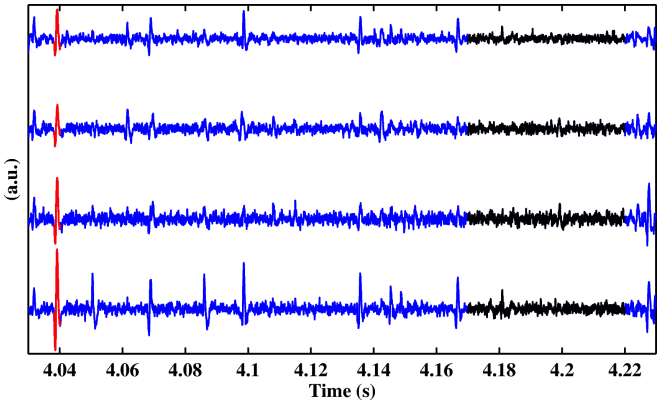

Fig. 1. The traces represent 200 ms of tetrode data ($c = 4$). One of the 20 manually selected EAPs is highlighted in red (duration 2 ms). A 50-ms-segment containing noise-only data is shown in black.

B. Approximate Generalized Matched Filter

Based on a typical EAP duration, we assumed a signal length of 2 ms ($l = 31$). For each noise segment and each sensor pair $\{i = 1, 2, 3, 4;\ j \geq i\}$, cross- and auto-covariance sequences, $r_{i,j}(k)$, were calculated at lags $k \in [-30, 30]$. These sequences were then averaged over the 25 noise segments to obtain stable estimates. Note that unlike auto-covariance, cross-covariance is not guaranteed to be an even function, although the values of $r_{i,j}(k)$ and $r_{i,j}(-k)$ were very close. Therefore, the cross-covariance sequences were averaged over the positive and negative lags, i.e. $\bar{r}_{i,j}(k) = 0.5\,[r_{i,j}(k) + r_{i,j}(-k)]$, $k \in [0, 30]$, resulting in a total of 310 (31×10) parameters. Finally, the p-values of $\bar{r}_{i,j}(k)$ were estimated by a Monte-Carlo simulation, and those $\bar{r}_{i,j}(k)$ deemed statistically insignificant (p$\geq$0.05) were set to 0. This further reduced the number of parameters to 269. Toeplitz matrices, $\boldsymbol{\Sigma}_{i,j}$, were then created and used as the building blocks of $\boldsymbol{\Sigma}$ (see Fig. 2). Note that $\boldsymbol{\Sigma}_{j,i} = \boldsymbol{\Sigma}_{i,j}^{\mathrm{T}}$.

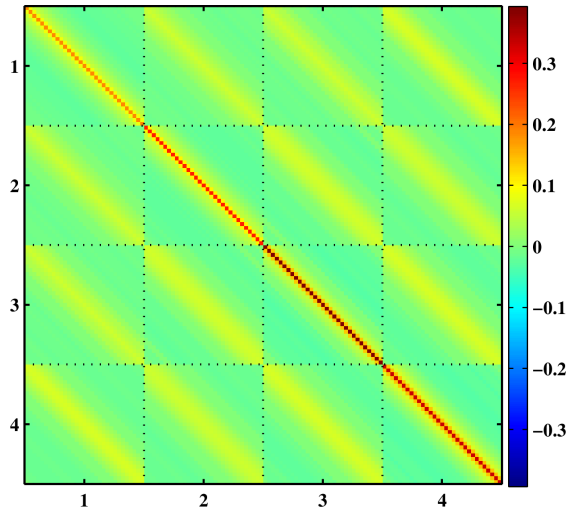

Fig. 2. The spatio-temporal noise covariance matrix, $\boldsymbol{\Sigma}$. Each block, $\boldsymbol{\Sigma}_{i,j} \in \mathbb{R}^{31\times31}$, is either the temporal covariance matrix of sensor i ($j = i$), or the temporal cross-covariance matrix between sensors i and j ($j \neq i$).

Biorthogonal wavelets (bior1.5[1]) were chosen due to their EAP-like shape (Fig. 3). The scale a was chosen so that the duration of the dominant two phases of the wavelet matches that of an EAP. For many EAPs, this falls between 0.5 and 2 ms [14], [15], thus 16 scales were chosen to cover the $[0.5, 2.0]$ ms range in 0.1-ms increments. Fig. 3 shows the wavelet function whose scale matches a 1-ms-long EAP. It also shows the basis vectors (5) at this scale.

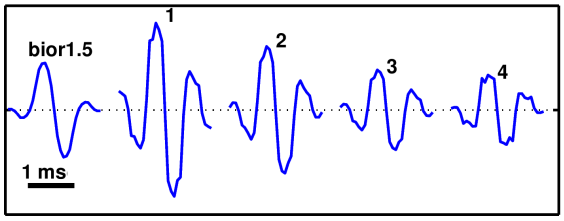

Fig. 3. Wavelet function and the basis vectors for sensors 1–4.

C. Signal-to-Noise Ratio

For each selected EAP, $\boldsymbol{S}^{(u)} \in \mathbb{R}^{4\times31}$ ($u = 1, 2, \cdots, 20$), and noise segment, $\boldsymbol{N}^{(v)} \in \mathbb{R}^{4\times d_v}$ ($v = 1, 2, \cdots, 25$; d_v-variable), the SNR at sensor i was defined as:

$$\mathrm{SNR}_i(u) = \underset{v}{\mathrm{median}} \left\{ \frac{\|\boldsymbol{s}_i^{(u)}\|_\infty}{\|\boldsymbol{n}_i^{(v)}\|_\infty} \right\} \qquad (6)$$

[1]The notation is consistent with MATLAB™Wavelet Toolbox.

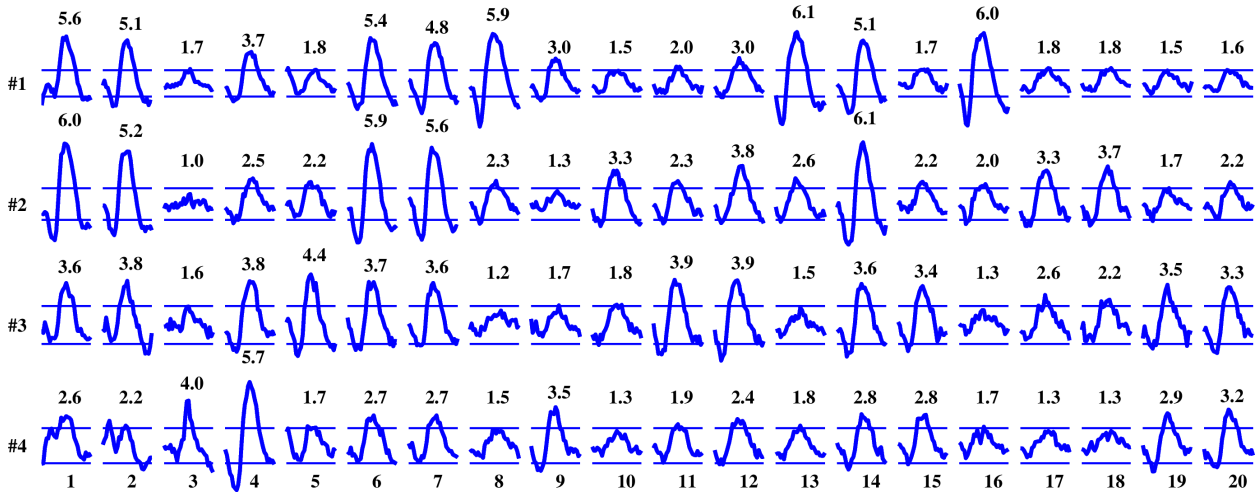

Fig. 4. A sample of 20 EAPs recorded with a tetrode (EAPs labeled 1-20, sensors labeled 1-4). Each trace is 2 ms long. The horizontal lines mark $\pm 5\sigma$ bounds, and the number next to each waveform represents its median SNR.

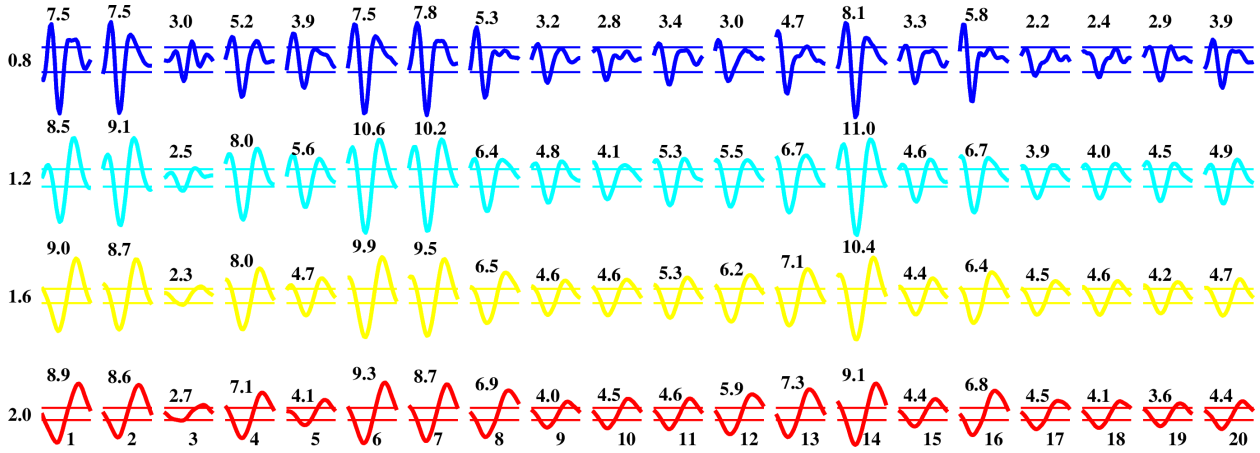

Fig. 5. Test statistic of 20 EAPs at 4 wavelet scales corresponding to the durations 0.8, 1.4, 1.6 and 2.0 ms. Each trace is 2 ms long. The horizontal lines mark $\pm 5\sigma$ bounds estimated from the test statistic of noise, and the number above each waveform represents its median SNR.

where $\boldsymbol{s}_i^{(u)}$ and $\boldsymbol{n}_i^{(v)}$ are the ith rows of matrices $\boldsymbol{S}^{(u)}$ and $\boldsymbol{N}^{(v)}$, respectively. Note that since nearly all detectors are threshold based, the SNR is more appropriately defined using the L^∞-norm than the commonly used L^2-norm. Apart from scaling the SNR values, the use of the L^2-norm did not affect the results presented below.

Fig. 4 shows the selected EAPs as well as the distribution of the SNRs across EAPs and sensors. Visual inspection confirms the diversity of the sample, as there appears to be at least 6 distinct classes of EAPs. The average SNR ranged from $\sim$2 (EAPs 3 and 10) to $\sim$4.5 (EAPs 1 and 6). Also shown are the noise bounds estimated by averaging the noise standard deviation over the 25 noise segments.

Fig. 5 shows a similar plot for the data processed using the procedure described in Section III. Briefly, for each of the 16 scales, the 4 basis vectors (e.g. Fig. 3) were flipped and convolved with their respective sensor data. The resulting test statistics were summed over sensors, yielding the test statistic sequence, $T_a(\mathcal{T}) \in \mathbb{R}^{1\times 30000}$, $(a = a_1, a_2, \cdots, a_{16})$. From the samples of $T_a(\mathcal{T})$ corresponding to EAPs and noise segments, the SNRs were calculated from (6), while formally replacing sensors, i, with scales, a. In the interest of space, Fig. 5 shows the EAP test statistic at 4 representative scales. Even from this reduced set of scales, it is apparent that substantial SNR improvements are achieved by the AGMF.

To formally ascertain the degree of SNR improvement, we performed statistical tests on the SNR of 20 EAPs. The maximum SNR per sensor was calculated for each of the 20 EAPs in the original data, yielding the following sequence of SNRs: $6.0, 5.2, \cdots, 3.3$ (see Fig. 4). Similarly, the maximum SNR per scale was calculated for each EAP in the AGMF-processed data (see Fig. 6). A sign test showed that the SNRs of the processed EAPs were significantly superior to those of the original data ($p<0.00004$), with a median improvement of 38%. A similar test was performed to compare the maximum SNR per sensor to the SNRs at the 16 individual scales (i.e. without taking the maximum over scales). It was found that the SNRs at 10 scales (1.1–2.0 ms) were superior to the maximum SNR based on the original data. These results indicate that even if the analysis is performed at a

single wavelet scale, the SNR improvements with respect to the original data are significant (Fig. 6). This figure also shows the distribution of SNRs across EAPs achieved with the power method [9], [11] and spatial prewhitening [10]. The power method was implemented by calculating the root-mean-square value of the data at each sensor in a 2-ms sliding window. The SNR on a per sensor basis was then calculated using (6). Finally, the spatial prewhitening method was implemented by averaging the spatial covariance matrix over 25 noise segments. The resulting matrix, $\mathbf{\Sigma}_s \in \mathbb{R}^{4\times4}$, was then spectrally decomposed, and the prewhitening matrix $\mathbf{\Sigma}_s^{-1/2}$ was calculated [21] and used to premultiply the tetrode data. As expected (see Fig. 6), a sign test showed that the SNR of the power method was significantly superior to the original SNR ($p<0.0004$), with a median improvement of 22%. The SNR of the prewhitening method, however, was inferior to the original SNR ($p<2\times10^{-6}$), with a median loss of 10%. In addition, both the power and prewhitening methods were significantly inferior to the AGMF method, with $p<0.01$ and $p<0.00004$, respectively, and a median loss of 18% and 35%, respectively.

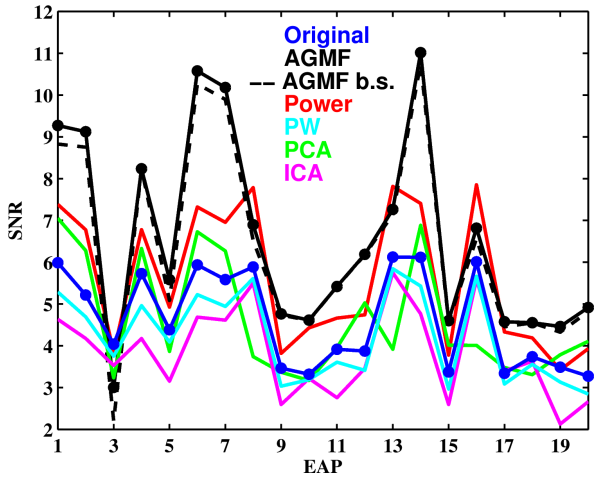

Fig. 6. Maximum (per sensor) SNR of the original, power, and spatially prewhitened (PW) data. Maximum (per scale) and best scale (b.s.) SNR of the AGMF-processed data. Maximum (per component) SNR of the PCA- and ICA-processed data.

We conclude this section by comparing the above methods to two popular unsupervised techniques: principal and independent component analysis (PCA and ICA, respectively). PCA yielded a median SNR improvement of 6% with respect to the original data, however, this gain was not statistically significant. ICA, on the other hand, resulted in a significant loss (20%) of SNR with respect to the original data.

V. Discussion and Conclusion

By combining statistical detection theory with continuous wavelet representation, we derived an approximation of the generalized matched filter suitable for semi-supervised EAP detection problems, where the noise samples are available, but the signal samples are not. The method outperforms other multisensor EAP detection approaches by yielding a significantly higher SNR when tested on representative EAPs and noise extracted from experimental data. A notable exception is EAP 3, which is characterized by the weak signals at 3 sensors (Fig. 4). This is hardly surprising as the test statistic, $T_{a,b}(\underline{\boldsymbol{x}})$, combines data across sensors, which in this case "dilutes" the SNR. Our work also shows that the use of *ad hoc* multisensor data processing methods may not only fail to improve the SNR, but may actually lower it. Future studies will focus on a formal testing of the AGMF method for the detection of EAPs under different sensitivity-specificity tradeoffs and in the presence of EAPs with temporal overlap. Finally, we will also pursue the development of a fully unsupervised multisensor EAP detection method.

References

[1] R.A. Andersen and H. Cui. Intention, action planning, and decision making in parietal-frontal circuits. *Neuron*, 63(5):568–583, 2009.

[2] R.Q. Quiroga, L. Reddy, G. Kreiman, C. Koch, and I. Fried. Invariant visual representation by single neurons in the human brain. *Nature*, 435(7045):1102–1107, 2005.

[3] J.A. White, J.T. Rubinstein, and A.R. Kay. Channel noise in neurons. *Trends Neurosci.*, 23(3):131–137, 2000.

[4] S.N. Gozani and J.P. Miller. Optimal discrimination and classification of neuronal action potential waveforms from multiunit, multichannel recordings using software-based linear filters. *IEEE Trans. Biomed. Eng.*, 41(4):358–372, 1994.

[5] M.A. Wilson and B.L. McNaughton. Dynamics of the hippocampal ensemble code for space. *Science*, 261(5124):1055–1058, 1993.

[6] S.G. Mallat. *A Wavelet Tour of Signal Processing*. Academic Press, San Diego, CA, 1999.

[7] Z. Nenadic and J.W. Burdick. Spike detection using the continuous wavelet transform. *IEEE Trans. Biomed. Eng.*, 52(1):74–87, 2005.

[8] R. Benitez and Z. Nenadic. Robust unsupervised detection of action potentials with probabilistic models. *IEEE Trans. Biomed. Eng.*, 55(4):1344–1354, 2008.

[9] J. Csicsvari, H. Hirase, A. Czurko, and G. Buzsáki. Reliability and state dependence of pyramidal cell-interneuron synapses in the hippocampus: an ensemble approach in the behaving rat. *Neuron*, 21(1):179–189, 1998.

[10] M. Sahani. *Latent Variable Models for Neural Data Analysis*. PhD thesis, California Institute of Technology, 1999.

[11] K.D. Harris, D.A. Henze, J. Csicsvari, H. Hirase, and G. Buzsáki. Accuracy of tetrode spike separation as determined by simultaneous intracellular and extracellular measurements. *J. Neurophysiol.*, 84(1):401–414, 2000.

[12] S.M. Kay. *Fundamentals of Statistical Signal Processing: Detection Theory*. Prentice-Hall, Englewood Cliffs, NJ, 1998.

[13] H.L. Van Trees. *Detection, Estimation and Modulation Theory*. Appleton & Lange, New York, 1991.

[14] D.R. Humphrey. *Electrophysiological Techniques*. Society for Neuroscience, Atlanta, 1979.

[15] R. Lemon. *Methods for Neuronal Recording in Conscious Animals*. Wiley, New York, 1984.

[16] X. Yang and S.A. Shamma. A totally automated system for the detection and classification of neural spikes. *IEEE Trans. Biomed. Eng.*, 35(10):806–816, 1988.

[17] K.G. Oweiss. *Multiresolution Analysis of Multichannel Neural Recordings in the Context of Signal Detection, Estimation, Classification and Noise Suppression*. PhD thesis, U. of Michigan, 2002.

[18] C. Pouzat, O. Mazor, and G. Laurent. Using noise signature to optimize spike-sorting and to assess neuronal classification quality. *J. Neurosci. Methods*, 122(1):43–57, 2002.

[19] K.L. Drake, K.D. Wise, J. Farraye, D.J. Anderson, and S.L. BeMent. Performance of planar multisite microprobes in recording extracellular single-unit intracortical activity. *IEEE Trans. Biomed. Eng.*, 35(9):719–732, 1988.

[20] C. Pouzat and G. Laurent. Locust data. Available online, http://www.biomedicale.univ-paris5.fr/SpikeOMatic/Data.html 2005.

[21] S.C. Wu, A.L. Swindlehurst, P.T. Wang, and Z. Nenadic. Projection versus prewhitening for EEG interference suppression. *IEEE Trans. Biomed. Eng.*, 59(5):1329–1338, 2012.